Karlsruher Institut für Technologie

FAKULTÄT FÜR PHYSIK

PHYSIKALISCHES PRAKTIKUM FÜR FORTGESCHRITTENE

PRAKTIKUM MODERNE PHYSIK

Gruppe Nr. 162 Kurs: ~~**Mo1**~~ **Mo2** **Mi3** 5

zutreffendes bitte ankreuzen — aktuelles Semester angeben

Versuch: Compton effect

Namen: Jonah Stier (uifed@student.kit.edu)

Hao Hu (hao.hu@student.kit.edu)

Assistent:

durchgeführt am: 20.11.2024

Protokollabgabe am:

vom Betreuer auszufüllen

Note gesamt [+] [0] [-]

Anerkannt:

(Datum Unterschrift)

Datum Rückgabe:

Bemerkung:

Contents

1 Objective of the Experiment, Theoretical Background[1]

1.1 Introduction

In nuclear and particle physics, scattering experiments are essential tools for studying the interactions between particles.All these scattering processes obey the laws of energy and momentum conservation, and under specific conditions, may also involve parity changes. This experiment focuses on elastic scattering, specifically the Compton effect, to investigate the exchange of energy and momentum between photons and electrons and validate the theoretical framework governing this interaction.
The Compton effect describes the interaction between photons and electrons, shedding light on the fundamental exchange of energy and momentum between photons and matter. We consider a photon of initial energy $E = h\nu$ and momentum $\vec{p} = \frac{h\nu}{c}$, where h is Planck's constant, ν is the frequency of the photon, and c is the speed of light. The photon collides with a stationary electron of mass m_e and initial energy $E_e = m_e c^2$. After the interactionthe photon is scattered at an angle θ relative to its initial direction with reduced energy $E' = h\nu'$and the electron recoils with a velocity $\vec{v}$ at an angle ϕ relative to the initial photon direction.
We apply the conservation laws of energy and momentum to this system.The total energy before and after the collision must remain the same:

$$E + E_e = E' + E'_e,$$

The momentum of the system is conserved in both the x- and y-directions. Representing the momenta as vectors:
1. In the x-direction:

$$\frac{h\nu}{c} = \frac{h\nu'}{c}\cos\theta + p_e \cos\phi.$$

2. In the y-direction:

$$0 = \frac{h\nu'}{c}\sin\theta - p_e \sin\phi.$$

Here, p_e is the magnitude of the electron's momentum after the collision.
To eliminate the electron's momentum and derive a direct relation between E, E', and θ, we use the invariants of the relativistic system. The key step involves the relativistic dot product of the four-momenta before and after the collision. Simplifying the relations yields:

$$\frac{1}{E'} - \frac{1}{E} = \frac{1}{m_e c^2}(1 - \cos\theta).$$

Rewriting in terms of the photon's wavelength ($\lambda = \frac{hc}{E}$):

$$\lambda' - \lambda = \frac{h}{m_e c}(1 - \cos\theta).$$

This is the Compton formula, which describes the shift in the wavelength ($\Delta\lambda = \lambda' - \lambda$) of a photon as a function of the scattering angle θ. The quantity $\frac{h}{m_e c}$ is known as the Compton wavelength of the electron (λ_C):

$$\Delta\lambda = \lambda_C(1 - \cos\theta).$$

[1] partially translated with Chat-GPt 4o and checked

From the derived Compton formula, it is evident that the wavelength shift of the photon is directly dependent on the scattering angle θ. When $\theta = 0°$, $\cos\theta = 1$, resulting in $\Delta\lambda = 0$, which indicates that the photon does not transfer any energy. Conversely, when $\theta = 180°$ (backscattering), $\cos\theta = -1$, the wavelength shift reaches its maximum value, $\Delta\lambda_{\max} = 2\lambda_C$, corresponding to the maximum energy transfer from the photon to the electron. However, even in this scenario, the photon's total energy is not fully transferred to the electron. This limitation arises because both energy and momentum conservation must be satisfied during the scattering process.

1.2 Scattering Cross Section

In experimental practice, it is often impossible to directly measure the momentum or wavelength of particles before and after a collision. Instead, the concept of the scattering cross section is introduced to quantify the likelihood of a scattering event occurring. The scattering cross section provides a measure of the effective area over which an incoming particle interacts with a target particle, offering a statistical representation of the interaction probability.
If the projectile interacts with this surface, the reaction occurs. The probability P_1 of such an interaction is given by:

$$P_1 = \frac{\sigma}{F},$$

where F is the area through which the projectile passes. If there are n target particles within the area, the probability of an impact becomes:

$$P_n = \frac{\sigma \cdot n}{F}.$$

The overall reaction rate R is determined by the probability of the event and the number of projectiles passing through the surface, expressed as:

$$R = P_n \cdot \Phi_0 \cdot F,$$

where Φ_0 is the flux of the incoming particles. Consequently, the scattering cross section can be calculated as:

$$\sigma = \frac{R}{n \cdot \Phi_0}.$$

An alternative form of the cross section, considering the reduced flux Φ_R after interaction, is given by:

$$\sigma = \frac{\Phi_R \cdot F}{\Phi_0 \cdot n} = \frac{\Phi_R}{\Phi_0} \cdot \frac{1}{n/F}.$$

To gain more detailed insight into the reaction, the differential cross section is introduced, which accounts for the probability of scattering within a specific solid angle $d\Omega$. This is expressed as:

$$\sigma = \frac{\text{energy flux per solid angle } d\Omega}{\text{incident energy flux} \times \text{number of target particles per unit area}}.$$

The total effective cross section is obtained by integrating the differential cross section over all directions:

$$\sigma = \int_0^{2\pi} d\phi \int_0^{\pi} \frac{d\sigma(\theta)}{d\Omega} \sin\theta \, d\theta.$$

In cases of isotropic scattering, the integral simplifies to:

$$\sigma = 2\pi \int_0^{\pi} \frac{d\sigma(\theta)}{d\Omega} \, d(\cos\theta).$$

1.3 Measurement of Photon Energy

In this experiment, the energy of the photon is measured using a scintillator detector. When a photon interacts with the scintillator, it transfers part of its energy to the electron through Compton scattering. These interactions may also generate additional low-energy photons or free electrons. Subsequently, these particles undergo further interactions, including Bremsstrahlung, resulting in a 'shower' of low-energy photons.
This photon 'shower' is ultimately detected by a photomultiplier tube (PMT), which converts it into an electrical signal. The magnitude of the electrical signal is proportional to the number of photons detected, and the number of photons is directly proportional to the energy transferred to the electrons. By analyzing the magnitude of this signal, we can indirectly determine the energy of the incident photon.
In the context of Compton scattering, at a specific angle, a sharp edge appears in the spectrum, corresponding to the case where the photon transfers its maximum energy to the electron through Compton scattering. Beyond this maximum energy, a sharp peak, known as the 'photopeak', appears in the spectrum, indicating that the photon has transferred all of its energy to the electron. By analyzing this information, we can determine the outcome of the scattering process and infer some of the details that may have occurred during the interaction.

2 Experimental Setup[1]

This experiment is divided into four interconnected tasks that are performed step by step. Each task builds upon the previous one, allowing for a comprehensive understanding of the Compton scattering process and the measurement techniques involved.

2.1 Energy Calibration and Detection Efficiency

Task 1 focuses on calibrating the data acquisition system and evaluating the detection efficiency of the entire setup. The primary components of the detector include a $CeBr_3$ scintillator and a photomultiplier tube (PMT), both mounted within a housing that is capable of rotation. The photomultiplier tube captures the light produced by the scintillator when it absorbs energy from the incoming photons. The resulting signal is then processed and digitized by a high-speed analog-to-digital converter (ADC).
An aluminum scattering target is positioned above the rotation axis of the detector, allowing for controlled variation of the scattering angle throughout the experiment. The digitized pulse signals are transmitted to a Linux-based PC, where they are stored for later processing. This pulse height is then converted into energy units through an energy calibration procedure. The calibration is performed using well-known photon sources ^{137}Cs, ^{60}Co, ^{57}Co, and ^{22}Na, whose photon energies are precisely known. The measured pulse heights are plotted against the known energies to establish a conversion formula between the ADC channel values and photon energies. In addition to the energy calibration, the detection efficiency of the system is determined by comparing the number of detected events to the expected events based on the known activity of the sources. This process ensures that the system's response is accurately characterized and can be applied to the measurements in subsequent tasks.

2.2 Differential Cross Section about angle

After completing the energy calibration and determining the detection efficiency, the experiment proceeds with measuring Compton scattering using a monoenergetic γ-ray source (^{137}Cs) and a cylindrical aluminum target. The detector is positioned at a fixed solid angle $\Delta\Omega$ relative to the target and can rotate around the target. The scattering angle θ is varied in steps of 15°, starting from 25°, with five different angles measured to observe scattering events at different angles.
For each scattering angle, two measurements are performed: first, the total photon detection rate, $R_T(\Delta\Omega, \theta)$, is recorded when the aluminum target is placed in front of the source; second, the background rate, $R_B(\Delta\Omega, \theta)$, is measured when the aluminum target is absent. The actual scattering rate in the aluminum target is calculated as the difference:

$$R_{\mathrm{Al}}(\Delta\Omega, \theta) = R_T(\Delta\Omega, \theta) - R_B(\Delta\Omega, \theta). \tag{2.1}$$

To determine the differential cross section, the following equation is used:

$$\frac{d\sigma}{d\Omega} = \frac{R(\Delta\Omega)}{\Delta\Omega} \cdot \frac{1}{\Phi_0 \cdot n \cdot \epsilon},$$

[1] partially translated with Chat-GPt 4o and checked

where Φ_0 is the flux of ^{137}Cs photons, n is the number of electrons in the target, and ϵ is the detector efficiency. The efficiency is a correction factor, which is determined experimentally as part of Task 1.
The number of electrons n in the aluminum target is calculated based on its geometric parameters:

$$n = \frac{N_A \cdot A \cdot Z \cdot \rho \cdot \pi \cdot (d/2)^2 \cdot l}{A},$$

where N_A is Avogadro's constant, A is the atomic mass of aluminum, Z is the atomic number, ρ is the density of aluminum, d is the diameter of the target, and l is the length of the target.
Finally, the solid angle $\Delta\Omega$ is calculated based on the experimental setup. By analyzing the photon detection rates at different scattering angles and applying the appropriate correction factors, the differential cross section is determined.

2.3 Energy Shift and Electron's Rest Energy

In Task 3, the goal is to measure the energy shift of the scattered γ-quanta as a function of the scattering angle and to estimate the electron's rest mass. According to the Compton scattering formula, the energy E' of the scattered photon can be expressed as a function of its initial energy E and the scattering angle θ:

$$\frac{1}{E'} = \frac{1}{E} + \frac{1}{m_0 c^2} \cdot (1 - \cos\theta),$$

where $m_0 c^2$ represents the rest energy of the electron. This equation shows that plotting $\frac{1}{E'}$ against $(1 - \cos\theta)$ yields a straight line, with the slope related to the electron's rest energy.
To perform the measurement, the energy E' of the scattered photons is determined by analyzing the photop peak in the energy spectrum at various scattering angles. Prior to this, the data acquisition system is calibrated using the known photon peaks from sources such as ^{22}Na, ^{57}Co, ^{60}Co, and ^{137}Cs, ensuring that the energy values are accurately recorded. The slope of the plot of $\frac{1}{E'}$ vs. $(1 - \cos\theta)$ will then provide the value of the electron's rest mass.

2.4 Dependence of the Effective Cross Section on the Atomic Number

In Task 4, the objective is to investigate how the effective cross section for Compton scattering depends on the atomic number Z of the target material. While the cross section in previous tasks was related to a free electron, when comparing different materials For large photon energies, where the binding energies of electrons are negligible, the following relation holds:

$$\left.\frac{d\sigma}{d\Omega}\right|_a = Z \cdot \left.\frac{d\sigma}{d\Omega}\right|_e,$$

where a and e represent the atom and the electron, respectively.
Using the equation for the electron's cross section and the relationship for the atomic cross section, we have:

$$\left.\frac{d\sigma}{d\Omega}\right|_e = C \cdot \frac{R \cdot A}{\rho \cdot Z},$$

C is a obvious constant . To verify this relationship, the scattering processes for aluminum, iron, and copper targets need to be measured, and the linear relationship between the differential cross section and atomic number should be determined from the experimental data.

3 Execution[1]

3.1 Energy calibration

For the energy calibration, the samples were placed directly in front of the detector and the spectrum was then measured for five minutes in each. The resulting histogram was displayed. Since the measurement did not measure the energy of the γ quantum but the photons converted by the scintillator or the maxima of the moving average of the voltage at the photomultiplier in channels of the analog-to-digital converter, the energy must be calibrated. A normal distribution was fitted to the photo peak. The expected values obtained in this way were plotted against the known energies of the isotopes which could be retrieved from the energy level schemes in the "blue book". A straight line was fitted to them. The standard deviation of the normal distribution was used as the error of the channel. There was no mention of the errors of the energy. The error is probably negligible as its small in relation to the standard deviation of the peaks. With the help of this function, the channels can be converted into energies.

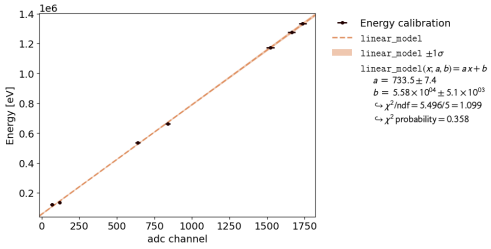

Figure 3.1: fit of the energy calibration

3.2 detection efficiency

The detector efficiency is the ratio of the events recorded by the detector, here specifically the events within a standard deviation around the expected value of the photo peak and the photons emitted by the source in the direction of the detector.
The detection efficiency can then be determined with $\epsilon = \frac{N_{\text{ph}}}{t_{\text{meas}} \cdot R_\gamma}$. Instead of the number of events the rate is used.
N_{ph} is the sum of the events, t_{meas} is the measurement time in seconds and R_γ is the rate of the incident γ quanta.
$R_\gamma = \phi_{\text{det}} \cdot A$ with $\phi_{\text{det}} = A_\gamma \frac{1}{4\pi l^2}$ where A_γ has decreased since the last measurement due to the decay.
A correction factor for the decay after t_{passed} years $A_\gamma = A_0 e^{-\frac{t_{\text{passed}} \cdot ln(2)}{t_{\frac{1}{2}}}}$ must be introduced.

$$\Rightarrow \epsilon = \frac{4 N_{\text{ph}} l^2}{t_{\text{meas}} A_0 r^2} e^{\left(ln(2) \frac{t_{\text{passed}}}{t_{\frac{1}{2}}} \right)}$$

Since Na_{22} decays with a probability of 90% in a $\beta+$ quantum and thus radiates through the recombination of positron and electron with two γ quanta, the activity for this decay must be

[1] partially translated with DeepL and checked

multiplied by 1.8. The γ emission to the ground state is not changed. Similarly, Cs_137 decays with 94.4% by emitting a γ photon, so its activity must be multiplied by 0.944.
The samples used with activity are shown below. The last measurement took place on 28.10.2024.

Table 3.1: Samples

Sample	Activity
Cs_{137} RP477	$2.58 \cdot 10^5\, Bq$
Co_{60} Ao2211	$4.01 \cdot 10^4\, Bq$
Na_{20} AC9255	$4.28 \cdot 10^3\, Bq$

The samples were now placed in the center of the arrangement, where the scattering target will also be placed later. The measurements were again carried out for five minutes, with the exception of Co_60, which was measured for ten minutes due to its low activity. Analogous to the energy calibration, a normal distribution was again fitted. Now all events within a standard deviation were summed. Since the Co_{60} and Na_{22} have two decays, the photo peak of the lower energy lies on the compton continuum of the higher energy. Therefore, the fit of the normal distribution, as well as the counting of the events is done with a constant offset. This procedure is only an approximation since the spectrum of the compton continuum is not flat (see 3.2(a)), but accurate enough.
The measurement of Co_{57} had to be discarded due to the premature removal of the sample and could not be repeated due to lack of time.

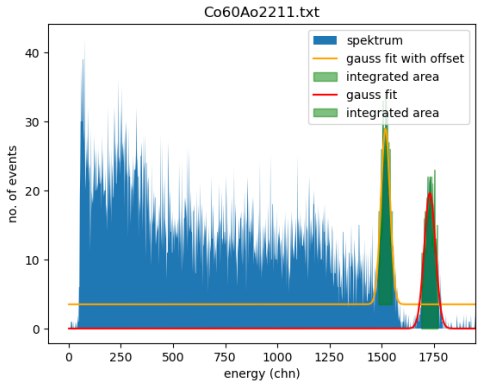

((a)) hist of Co_{60}

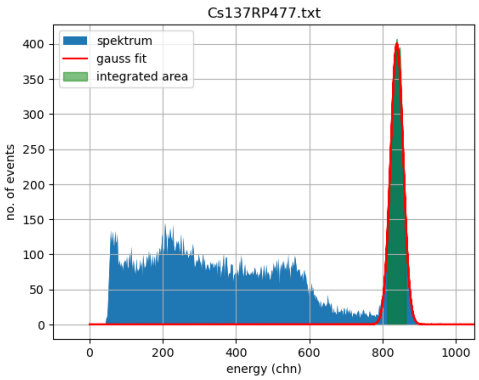

((b)) hist of Cs_{137}

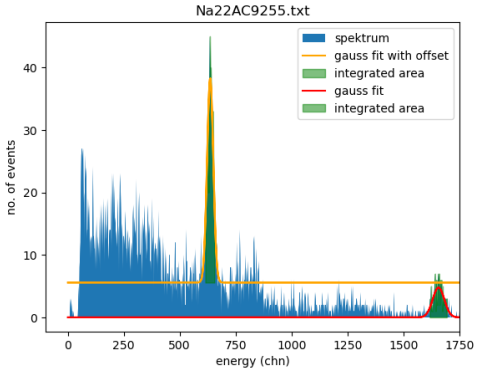

((c)) hist of Na_{22}

Figure 3.2: Display of the histogram of the samples as well as the normal distribution and the sum of the events

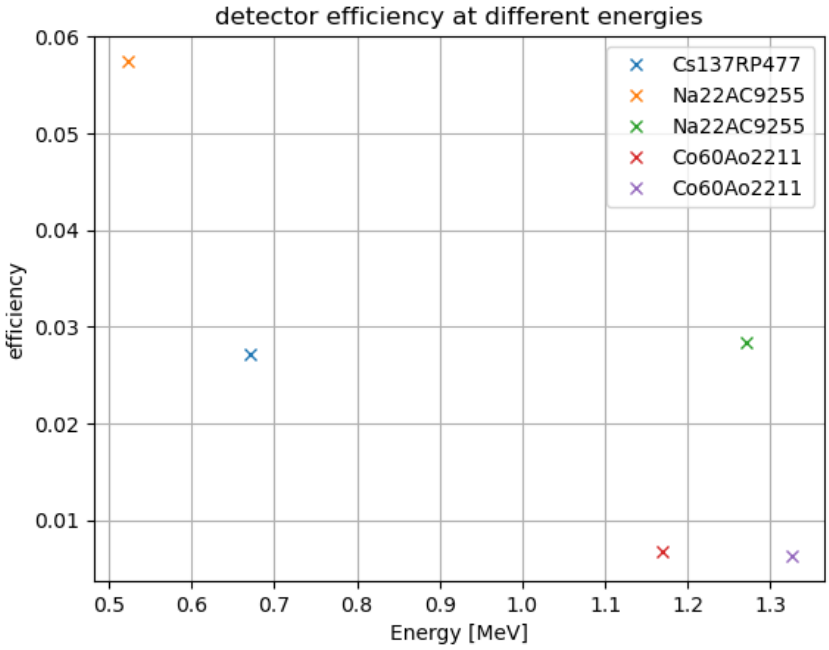

Figure 3.3: efficiency of the detector over energy

The calculated efficiency was plotted against the energy 3.3. It can be seen that the value for the γ transition of Na_{22} is higher than the surrounding values. One explanation would be that the correction factors are not correct. Since the value for the $\beta+$ decay seems to fit in well, a measurement error is ruled out. A function was fitted3.4 to this. The function used was an exponential function according to

$$f(E) = a \cdot e^{-b \cdot E} + c$$

as it is to be expected that the efficiency will continue to decrease for higher energies. The efficiency can then be interpolated using the function determined in this way.

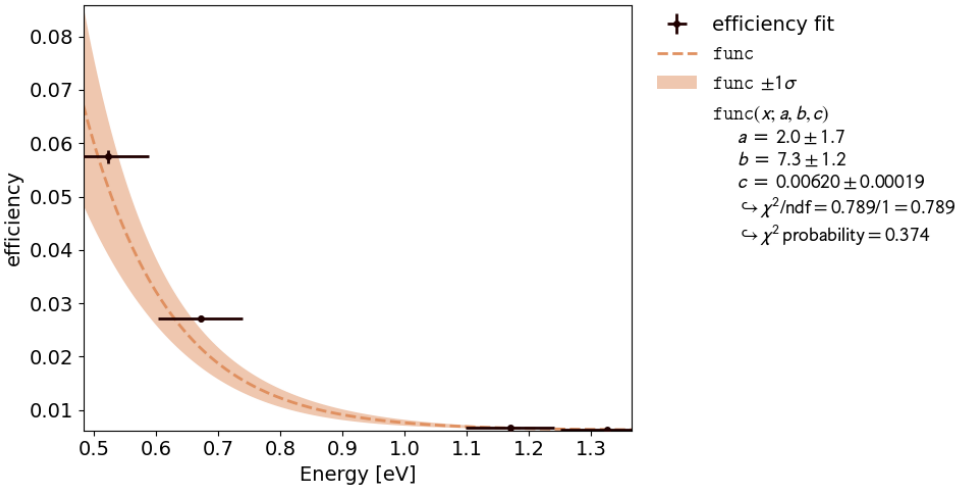

Figure 3.4: Fit of the efficiency

For the fit, the value for the γ-scaling of Na_{22} had to be omitted so that the fit converges.
The energy uncertainty and the uncertainties of the efficiencies propagated with the uncertainties module were used as uncertainties.

The efficiencies determined with the resulting function have a high uncertainty in the later relevant range between $\sim 0.3\,MeV$ and $\sim 0.7\,MeV$ which is due to the high energy uncertainty.

3.3 Differential Cross Section about angle

We started at a scattering angle of 25°, and measured the scattering data for 25°, 40°, 55°, 70°, and 85° with and without the aluminum target, using a step size of 15°. By subtracting the background data and applying the fitting method obtained in Task 1, we successfully determined the actual scattering rate for the aluminum target at different angles, as shown in the figure below.

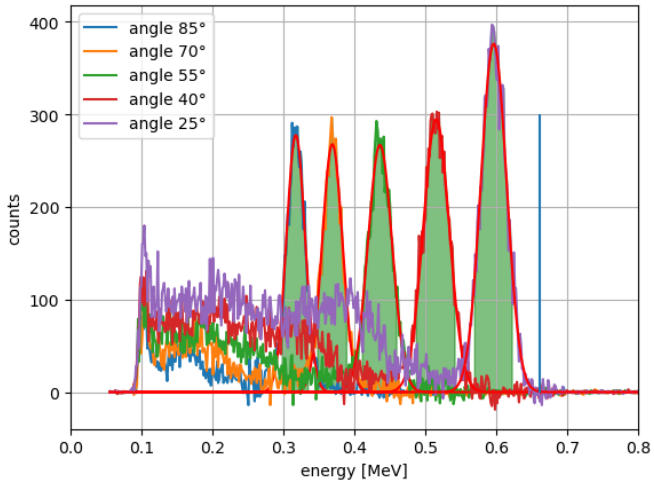

Figure 3.5: Actual scattering rate

Using formula 2.1, we calculated the differential scattering cross section at different angles from the obtained scattering rates. Here, ϵ is the detection efficiency obtained in Task 1 which is energy dependent. After substituting all the data, we obtained the relationship between the differential scattering cross section and the incident angle, as shown in the figure below.

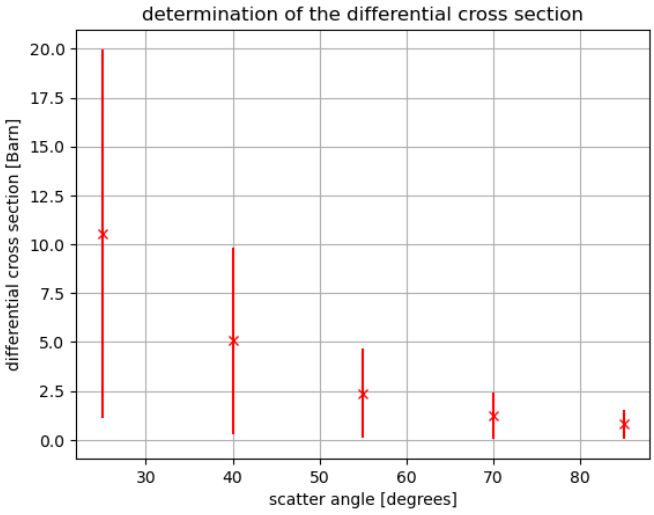

Figure 3.6: Relationship between the differential scattering cross section and the incident angle.

As shown in the figure, the differential scattering cross section decreases with increasing incident angle (from 25° to 85°). This can be attributed to two factors.
First, the kinematics of the Compton scattering process indicates that as the scattering angle increases, the energy transfer decreases, meaning that photons at higher angles interact less with

the electrons. Secondly, I suspect that the angular distribution of the scattered photons also contributes to this trend. At smaller angles, more photons scatter in the forward direction, leading to a higher cross section. At larger angles, the photon distribution becomes more spread out, and fewer photons scatter at higher angles, which also contributes to this result. Therefore, the differential scattering cross section decreases with increasing incident angle, reflecting the reduced interaction efficiency and scattering probability at larger angles, which is consistent with the experimental expectations.

3.4 electron mass

The energy shift is now used to determine the mass of the electron.
The energy E' of the γ photon after scattering as a function of the scattering angle is

$$\frac{1}{E'} = \frac{1}{E} - \frac{1}{m_0 c^2}(1 - cos(\theta))$$

The reciprocal energy is plotted against one minus the cosine of the scattering angle and a straight line is fitted to it. As error for the measured energy we use the standard deviation of the normal distribution of the photo peaks. The error of the angle is neglected as it's considered small. The slope of the line $(a)3.7$ is $\frac{1}{m_0 c^2}$. If we now form the reciprocal value and divide by the speed of light squared, we obtain the electron mass $m_0 = (9.8 \pm 3.5) \cdot 10^{-31}$ Kg. The literature value[2] $m_e = 9.1093837139 \cdot 10^{-31}$ Kg is within the range of uncertainty, though the uncertainty is great. This is caused by the high uncertainty of the energy.

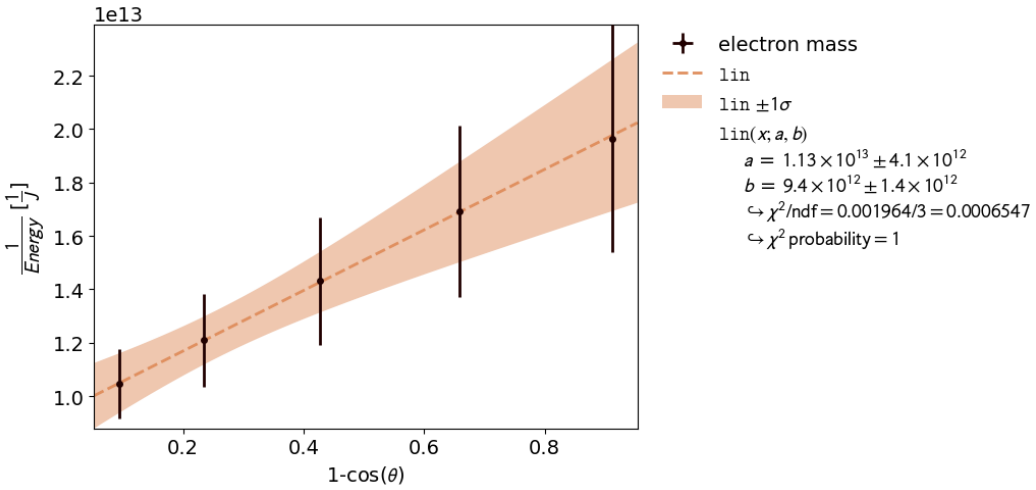

Figure 3.7: linear fit to determine the electron mass

The χ^2 probability is 1 and $\frac{\chi^2}{ndf} = 0.0006547$. Especially $\frac{\chi^2}{ndf}$ is very low. The fit itself is good, the obtained value has a high uncertainty. To reduce the uncertainty one would need a better detector to make the photo peaks slimmer.

3.5 Effective Cross Section about the Atomic Number

Finally, with the scattering angle fixed at 85°, we sequentially replaced the target with aluminum, iron, and copper, and performed scattering measurements for each material. Similar to the previous analysis, we first obtained the scattering rates with and without the target, and then subtracted the background rate to determine the actual scattering rates for each case, as shown in the figure below:

[2] `https://physics.nist.gov/cgi-bin/cuu/Value?me`

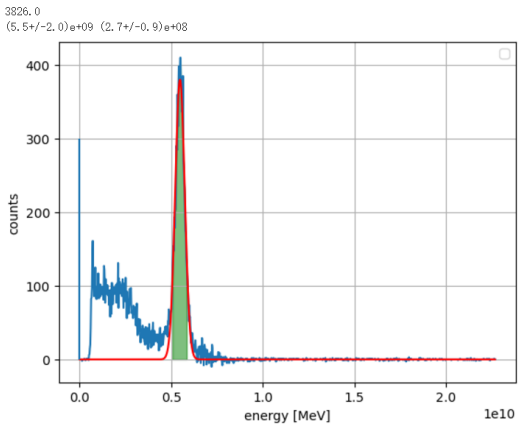

((a)) R for Aluminum

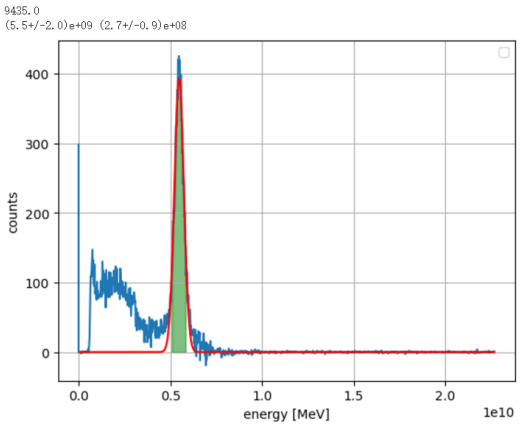

((b)) R for Iron

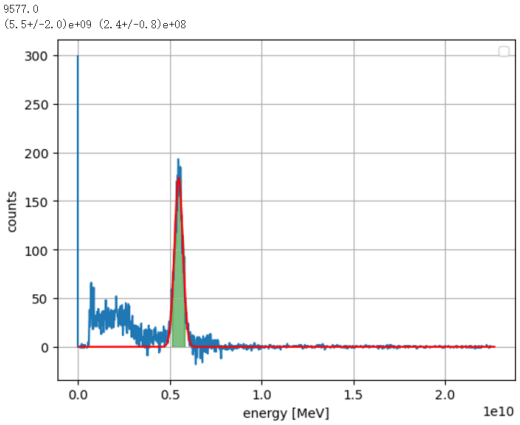

((c)) R for Copper

Subsequently, we calculated the differential scattering cross section for each material based on the scattering rates, and fitted the function relationship between $\frac{R \cdot A}{\rho}$ and the atomic number. The resulting fit shows an approximate linear relationship, as shown in the figure below:

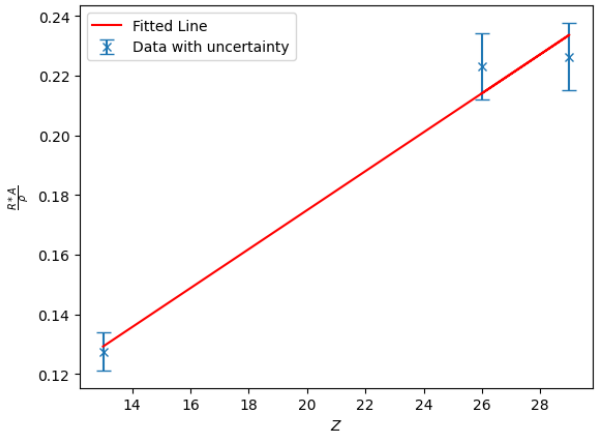

Figure 3.9: Fit of the function $\frac{R \cdot A}{\rho}$ versus the atomic number, showing an approximate linear relationship.

In this analysis, I applied a 2% uncertainty and performed a fitting correction. As can be seen, the data for iron deviates slightly from the straight line, but it still lies close to it. I suspect that this deviation might be due to the imprecision in our measurements, which led to some

discrepancies, causing the fitted linear function to not be perfectly accurate.
Another reason could be that the atomic numbers of the materials we measured are relatively close to each other. In principle, we should have measured materials with a larger atomic number, such as lead, so that the differences in the results would be more pronounced, and the measured data might be closer to the fitted linear function.

]Evaluation, error calculation and discussion of the measurement results